Multi-Dimensional Parachute Deployment Box for Mars Precision Landing

XING Zhehao[1, 2]，LIANG Zixuan[1, 2]

（1. School of Aerospace Engineering, Beijing Institute of Technology, Beijing 100081, China；
2. Key Laboratory of Autonomous Technology for Deep Space Exploration, Ministry of Industry and Information Technology, Beijing 100081, China）

Abstract： The parachute deployment conditions during the terminal entry phase in Mars landing missions exhibit critical impact on landing precision. In this article, aiming at the requirements of safe parachute deployment and accurate landing, a multi-dimensional parachute deployment box for determining deployment condition during Mars landing was proposed. First, an extreme-range optimization model was established, synthesizing the dynamics and constraints of both parachute descent and powered descent phases. Then, on the basis of the two-dimensional altitude-velocity deployment box, a multi-dimensional parachute deployment box characterized by altitude, velocity, flight-path angle, and extreme range was constructed through the integration of extreme range information. Furthermore, an evaluation index for landing precision was formulated and a deployment control logic was proposed for minimizing landing deviation. Finally, the proposed deployment box was simulated in a Mars landing mission. The results demonstrate that the proposed box effectively satisfies safe deployment and landing precision demands, eliminating the range-to-go error at the terminal of the entry phase.

Keywords： Mars exploration；precision landing；multiple constraints；parachute deployment box；parachute deployment control

Highlights：

- A multi-dimensional box is developed for determining parachute deployment conditions during Mars landing.
- The multi-dimensional box is constructed on the basis of the extreme-range optimization model and the two-dimensional box.
- The parachute deployment logic based on the multi-dimensional box is capable of increasing the landing precision.

中图分类号：V448.2　　文献标识码：A　　文章编号：2096-9287(2025)06-0629-10

DOI:10.3724/j.issn.2096-9287.2025.20250045

Reference format: XING Z H，LIANG Z X. Multi-dimensional parachute deployment box for Mars precision landing[J]. Journal of Deep Space Exploration, 2025, 12 (6) : 629-638.

引用格式：邢哲豪，梁子璇. 面向火星精确着陆的多维开伞窗口设计[J]. 深空探测学报（中英文），2025，12（6）：629-638.

Introduction

Mars exploration serves as a crucial approach for humans to unravel the mysteries of the universe, investigate the origins of life, and pursue extraterrestrial survival[1]. As engineering capabilities advance and scientific research deepens, in-situ exploration and sample return missions have emerged as focal points in Mars exploration[2-3]. Precise landing on Mars surfaces is a pivotal technology for both in-situ exploration and sample return missions. It determines whether the lander can reach the designated research areas on the Mars surface and forms the foundation for subsequent exploration activities[4-6].

Mars landing typically consists of three phases: the entry phase, the parachute descent phase, and the powered descent phase. Since the parachute descent phase is generally uncontrolled and the powered descent phase has limited control authority[7], the parachute deployment conditions at the terminal of the entry phase critically determines whether the lander can reach the desired landing site. Premature parachute deployment would prevent the lander from achieving the required flight range, causing early touchdown before reaching the target

收稿日期：2025-06-11　修回日期：2025-08-23

基金项目：Supported by the National Natural Science Foundation of China（62073034）

area. Conversely, delayed parachute deployment would result in the lander overshooting the target area. In addition to satisfying the range constraint, parachute deployment must comply with Mach number and dynamic pressure constraints to ensure safe ejection and inflation[8], as well as meet minimum altitude constraint to guarantee sufficient altitude for completing both parachute descent and powered descent phases[9]. Researchers commonly refer to the set of parachute deployment states satisfying these multiple constraints as the parachute deployment box[10], where violations of the box significantly increase failure risks of the mission. Therefore, developing multi-dimensional parachute deployment box is essential for achieving safe parachute deployment and precise landing.

Research on parachute deployment control methods for landers has been investigated in the past decades. Methods include time sequence method, acceleration-overload method, barometric altimetry method, radar altimetry method, and two-dimensional altitude-velocity box method[11]. Notably, time sequence method, acceleration overload method, and barometric altimetry method require the accurate planetary atmospheric model. These methods have been predominantly applied to Earth re-entry missions but face limitations in extraterrestrial landing missions with unknown or uncertain atmospheric conditions[12]. The radar altimetry method necessitates the installation of a height radar near the lander's heatshield, imposing stringent requirements on both the structural design and thermal protection capabilities of the heat shield. To date, only the Viking mission has implemented this method[13]. The two-dimensional altitude-velocity box method, which utilizes dynamic pressure, Mach number, and altitude as control parameters, demonstrates strong adaptability for planetary landing with uncertain environment. This method has been extensively employed in multiple Mars landing missions[14-18]. Fundamentally, this method evaluates whether the lander's states fall within the safe parachute deployment box. However, although states within this box satisfy safety requirements, it neglects the range-to-go information, thereby failing to guarantee landing precision within the target area. The Perseverance rover (Mars 2020) adopted a velocity-constrained downrange trigger. This system initiates velocity condition verification (permissible velocity interval is 370–573 m/s) only after the lander reaches a predetermined range-to-go threshold[19]. However, its reliance on pre-calibrated range-to-go threshold disregards real-time state dispersion during flight, resulting in significant velocity uncertainty during parachute deployment[20]. In summary, existing research on parachute deployment focuses primarily on meeting safety requirements, while the impact of deployment control on landing precision has received less attention. Therefore, an effective parachute deployment box must simultaneously prioritize parachute deployment safety and landing accuracy, moving beyond singular reliance on safety criteria to minimize landing errors while ensuring lander security.

In this article, aiming at the dual requirements of safe parachute deployment and precise landing in planetary landing process, a parachute deployment box for Mars landing is proposed. To ensure safe parachute deployment, a two-dimensional altitude-velocity box is established through dynamic pressure, Mach number, and altitude constraints, which is subsequently extended to a multi-dimensional parachute deployment box to guarantee all deployment states remain within safe operational boundaries. For landing precision enhancement, an extreme-range optimization model is developed to incorporate range information into the multi-dimensional box. The proposed deployment box effectively enhances landing accuracy while maintaining safe parachute deployment.

1 Dynamics and Constraints

A planet-fixed coordinate system O-XYZ is established as follows: the origin O is positioned at the planetary center. The OX-axis is directed toward the intersection of the equatorial plane and the prime meridian. The OZ-axis aligns with the rotational axis pointing toward the North Pole. The OY-axis completes the orthogonal triad according to the right-hand rule. The dynamics presented in this section are formulated within the planet-fixed coordinate system.

Due to Mars' slow rotation and the short landing duration, planetary rotation has a negligible effect. Considering the low initial altitude of the Mars lander at the terminal of the entry phase, gravitational acceleration remains effectively constant. Under the assumptions of

planetary rotation negligence and uniform gravitational acceleration, the dynamics of the lander at the terminal of the entry phase is formulated as

$$\begin{cases} \dot{r} = v\sin\gamma \\ \dot{\theta} = \dfrac{v\cos\gamma\sin\psi}{r\cos\phi} \\ \dot{\phi} = \dfrac{v\cos\gamma\cos\psi}{r} \\ \dot{v} = -D - g\sin\gamma \\ \dot{\gamma} = \dfrac{1}{v}\left(L\cos\sigma - g\cos\gamma + \dfrac{v^2\cos\gamma}{r}\right) \\ \dot{\psi} = \dfrac{L\sin\sigma}{v\cos\gamma} + \dfrac{v\cos\gamma\sin\psi\tan\phi}{r} \end{cases} \tag{1}$$

where r is the distance from the center of the planet to the lander, θ is the longitude, ϕ is the latitude, v is the velocity magnitude, γ is the flight-path angle, ψ is the velocity heading angle, g is the gravitational acceleration on Mars, and σ is the bank angle. L and D are the lift and drag acceleration before parachute deployment, respectively. The lift and drag acceleration are mathematically formulated as

$$\begin{cases} L = \dfrac{\rho v^2 S_{\mathrm{A}} C_{\mathrm{L}}}{2m_{\mathrm{e}}} \\ D = \dfrac{\rho v^2 S_{\mathrm{A}} C_{\mathrm{D}}}{2m_{\mathrm{e}}} \end{cases} \tag{2}$$

where m_{e} is the mass of the lander at the terminal of the entry phase, ρ is the atmospheric density, and S_{A} is the reference area of the lander before parachute deployment. C_{L} and C_{D} are the lift and drag coefficient of the lander before parachute deployment, respectively. The atmospheric density adopts an exponential model, which is expressed as

$$\rho = \rho_0 \mathrm{e}^{-h/h_s} \tag{3}$$

where ρ_0 is the atmospheric density on planet surface, h is the altitude of the lander, and h_s is the nominal density scale altitude.

The dynamic deployment process includes inflation, pneumatic flutter, and offloading. The duration of this process is very short[21] so that the impact can be neglected. Under the assumptions of planetary rotation negligence, uniform gravitational acceleration, and negligible disturbance (including inflation, pneumatic flutter, and offloading), the dynamics of the lander during the parachute descent phase is formulated as

$$\begin{cases} \dot{r} = v\sin\gamma,\ \dot{\theta} = \dfrac{v\cos\gamma\sin\psi}{r\cos\phi} \\ \dot{\phi} = \dfrac{v\cos\gamma\cos\psi}{r},\ \dot{v} = -\bar{D} - g\sin\gamma \\ \dot{\gamma} = \dfrac{1}{v}\left(\bar{L} - g\cos\gamma + \dfrac{v^2\cos\gamma}{r}\right) \\ \dot{\psi} = \dfrac{v\cos\gamma\sin\psi\tan\phi}{r} \end{cases} \tag{4}$$

where $\bar{L}$ and $\bar{D}$ are the lift and drag acceleration after parachute deployment, respectively, which are given by

$$\begin{cases} \bar{L} = \dfrac{\rho v^2 \bar{S}_{\mathrm{A}} \bar{C}_{\mathrm{L}}}{2m_{\mathrm{p}}} \\ \bar{D} = \dfrac{\rho v^2 \bar{S}_{\mathrm{A}} \bar{C}_{\mathrm{D}}}{2m_{\mathrm{p}}} \end{cases} \tag{5}$$

where m_{p} is the mass of the lander during the parachute descent phase, and $\bar{S}_{\mathrm{A}}$ is the reference area after parachute deployment. $\bar{C}_{\mathrm{L}}$ and $\bar{C}_{\mathrm{D}}$ are the lift and drag coefficient after parachute deployment, respectively.

During the parachute descent phase, the lander undergoes a sequence of discrete mass jettison events, including the separation of the heatshield, parachute compartment, and backshell. The jettison of the mass can be modeled by

$$\begin{cases} m_{\mathrm{p}}(v > v_{\mathrm{h}}) = m_{\mathrm{p}}(v \leqslant v_{\mathrm{h}}) + m_{\mathrm{h}} \\ m_{\mathrm{pf}} = m_{\mathrm{T0}} + m_{\mathrm{b}} \end{cases} \tag{6}$$

where m_{h} is the mass of the heatshield, v_{h} is velocity magnitude of the lander to separate the heatshield, m_{pf} is the mass of the lander during the terminal of the parachute descent phase, m_{T0} is the mass of the lander at the initial time of the powered descent phase, and m_{b} is the total mass of the parachute, parachute compartment, and backshell.

Under the assumptions of planetary rotation negligence, aerodynamic force negligence, and uniform gravitational acceleration, the dynamics of the lander during the powered descent phase is formulated as

$$\begin{cases} \dot{r} = v\sin\gamma,\ \dot{\theta} = \dfrac{v\cos\gamma\sin\psi}{r\cos\phi},\ \dot{\phi} = \dfrac{v\cos\gamma\cos\psi}{r} \\ \dot{v} = \dfrac{T}{m_{\mathrm{T}}}\left[\sin\gamma\cos\eta + \cos\gamma\sin\eta\cos(\chi - \psi)\right] - g\sin\gamma \\ \dot{\gamma} = \dfrac{T}{m_{\mathrm{T}} v}\left[\cos\gamma\cos\eta - \sin\gamma\sin\eta\cos(\chi - \psi)\right] - \\ \qquad \dfrac{g}{v}\cos\gamma + \dfrac{v}{r}\cos\gamma \\ \dot{\psi} = \dfrac{T\sin\eta\sin(\chi - \psi)}{m_{\mathrm{T}} v\cos\gamma} + \dfrac{v\cos\gamma\sin\psi\tan\phi}{r},\ \dot{m}_{\mathrm{T}} = -\dfrac{T}{I_{\mathrm{sp}} g_{\mathrm{E}}} \end{cases} \tag{7}$$

where m_T is the mass of the lander during the powered descent phase, T is the thrust magnitude, η is the thrust pitch angle, χ is the thrust heading angle, I_{sp} is the specific impulse of the thruster, and g_E is the value of the gravity acceleration at the Earth's sea level.

The thrust constraint during the powered descent phase is expressed as

$$T_{min} \leqslant T \leqslant T_{max} \tag{8}$$

where T_{min} and T_{max} are the maximum and minimum thrust magnitudes, respectively.

The mass constraint during the powered descent phase is expressed as

$$m_{T0} - m_{Tf} \geqslant m_{fuel} \tag{9}$$

where m_{Tf} is the mass of the lander after landing on the planet surface, and m_{fuel} is the mass of the fuel.

2 Multi-dimensional Box for Parachute Deployment

The multi-dimensional box for parachute deployment control is designed, as shown in Fig. 1. The parachute deployment stated within the multi-dimensional box ensures precise landing of the lander at the target site. To meet the requirements of safe parachute deployment and precision landing, an extreme-range optimization model is established. Extending from the classical two-dimensional box, a multi-dimensional parachute deployment box characterized by altitude, velocity, flight-path angle, and extreme range is constructed. Furthermore, an evaluation index for landing precision is formulated, and a control logic for parachute deployment is developed.

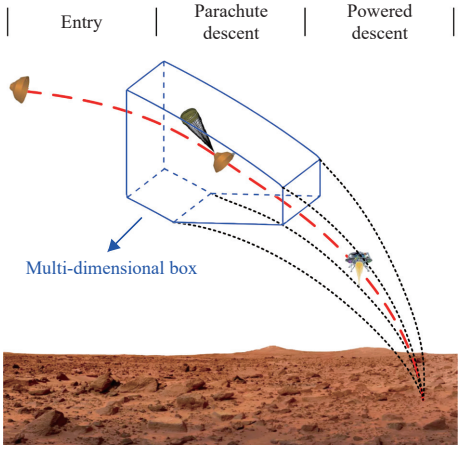

Fig. 1 Diagram of multi-dimensional parachute deployment box

2.1 Extreme-range Optimization Model

The extreme range is defined as the maximum and minimum reachable ranges from parachute deployment to touchdown. Generally, landers exhibit limited maneuverability in the parachute descent phase but exhibit enhanced maneuverability in the powered descent phase. Therefore, the difference between maximum and minimum reachable ranges after parachute deployment originates principally from the powered descent phase. The extreme-range optimization model solves thrust sequence to obtain the lander's maximum and minimum reachable ranges after parachute deployment.

The transition condition from the parachute descent phase to the powered descent phase is defined as follows: When the lander's altitude decreases to the threshold h_T, the parachute is jettisoned and the thrusters are ignited. The lander transitions from parachute descent to powered descent phase.

Incorporating the thrust constraint shown in Equation (8) and the mass constraint shown in Equation (9), a maximum-range optimization model is given by Equation (10), and a minimum-range optimization model is given by Equation (11):

$$\begin{aligned} &\max J_1 = S \\ &\text{s.t.} \begin{cases} \dot{\boldsymbol{X}} = \boldsymbol{F}_p(\boldsymbol{X}), \ \text{if} \ t_p \leqslant t \leqslant t_T \\ \dot{\boldsymbol{X}} = \boldsymbol{F}_T(\boldsymbol{X}), \ \text{if} \ t_T < t \leqslant t_f \\ h(t_p) = h_p, \ v(t_p) = v_p, \ \gamma(t_p) = \gamma_p \\ h(t_T) = h_T \\ h(t_f) = 0, \ v(t_f) = 0 \\ T_{min} \leqslant T \leqslant T_{max} \\ m_{T0} - m_{Tf} \geqslant m_{fuel} \end{cases} \end{aligned} \tag{10}$$

$$\begin{aligned} &\min J_2 = S \\ &\text{s.t.} \begin{cases} \dot{\boldsymbol{X}} = \boldsymbol{F}_p(\boldsymbol{X}), \ \text{if} \ t_p \leqslant t \leqslant t_T \\ \dot{\boldsymbol{X}} = \boldsymbol{F}_T(\boldsymbol{X}), \ \text{if} \ t_T < t \leqslant t_f \\ h(t_p) = h_p, \ v(t_p) = v_p, \ \gamma(t_p) = \gamma_p \\ h(t_T) = h_T \\ h(t_f) = 0, \ v(t_f) = 0 \\ T_{min} \leqslant T \leqslant T_{max} \\ m_{T0} - m_{Tf} \geqslant m_{fuel} \end{cases} \end{aligned} \tag{11}$$

where S is the range traversed by the lander from parachute deployment to touchdown, and $\boldsymbol{X} = [r, \theta, \phi, v, \gamma, \psi]^T$ is the state of the lander. $\boldsymbol{F}_p(\cdot)$ and $\boldsymbol{F}_T(\cdot)$ are the dynamics of the lander during the parachute descent phase

and the powered descent phase, respectively. t_{p}, t_{T}, and t_{f} are moment for parachute deployment, thrusters' ignition, and final touchdown, respectively. h_{p}, v_{p}, and γ_{p} are the altitude, velocity magnitude, and flight-path angle of the lander at the initial moment of the parachute descent phase, respectively.

The optimization problems formulated in Equations (10) and (11) can be transformed into convex forms[22], thereby achieving enhanced computational efficiency. The extreme-range optimization model can be solved by the convex optimization algorithm.

2.2 Construction of the Multi-dimensional Box

The classical two-dimensional parachute deployment box lacks range information, resulting in failure to accommodate precision landing requirements. To address this limitation, it is imperative to establish a multi-dimensional parachute deployment box that incorporates altitude, velocity, flight-path angle, and extreme range.

For safety reason, the deployment states for the parachute are constrained by Mach number, dynamic pressure, and altitude. The constraints are expressed as

$$\begin{cases} M_{\min} \leqslant M_{\mathrm{p}} \leqslant M_{\max} \\ q_{\min} \leqslant q_{\mathrm{p}} \leqslant q_{\max} \\ h_{\mathrm{p}} \geqslant h_{\min} \end{cases} \tag{12}$$

where $M_{\min}$ and $M_{\max}$ are the minimum and maximum Mach number, respectively. $q_{\min}$ and $q_{\max}$ are the minimum and maximum dynamic pressure, respectively. $h_{\min}$ is the minimum altitude. M_{p}, q_{p}, and h_{p} are the Mach number, dynamic pressure, and altitude for parachute deployment, respectively.

According to Equation (12), the classical two-dimensional box can be derived as

$$\begin{cases} h \geqslant h_{\min} \\ \max\left\{\sqrt{\dfrac{2q_{\min}}{\rho}}, c_h M_{\min}\right\} \leqslant v \leqslant \min\left\{\sqrt{\dfrac{2q_{\max}}{\rho}}, c_h M_{\max}\right\} \end{cases} \tag{13}$$

where c_h is the velocity of sound at altitude h.

Uniform sampling is conducted across the two-dimensional box, as demonstrated in Equation (14)

$$\begin{aligned} &\mathrm{sample}\,(h_{\mathrm{p}i}, v_{\mathrm{p}j}) \in W_1 \\ &\text{s.t.} \begin{cases} h_{\mathrm{p}i} = h_{\min} + i(h_{\max} - h_{\min})/n_h, & i = 0,1,2,\cdots,n_h \\ v_{\mathrm{p}j} = v_{\min} + j(v_{\max} - v_{\min})/n_v, & j = 0,1,2,\cdots,n_v \end{cases} \end{aligned} \tag{14}$$

where $(h_{\mathrm{p}i}, v_{\mathrm{p}j})$ is the sampling point, and W_1 is the two-dimensional box. $h_{\min}$ and $h_{\max}$ are the minimum and maximum altitude in the two-dimensional box, respectively. $v_{\min}$ and $v_{\max}$ are the minimum and maximum velocity in the two-dimensional box, respectively. n_h and n_v are positive integers.

For the sampling points in the two-dimensional box, different initial flight-path angles are taken by

$$\gamma_{\mathrm{p}k} = \gamma_{\min} + k(\gamma_{\max} - \gamma_{\min})/n_\gamma, \quad k = 0,1,2,\cdots n_\gamma \tag{15}$$

where $\gamma_{\min}$ and $\gamma_{\max}$ are the minimum and maximum initial flight-path angle, respectively. n_γ is a positive integer.

Based on Equation (14) and Equation (15), the state set of parachute deployment can be expressed by

$$B_{\mathrm{p}} = \{(h_{\mathrm{p}i}, v_{\mathrm{p}j}, \gamma_{\mathrm{p}k})\} \tag{16}$$

By taking elements from the parachute deployment state set B_{p} as the initial conditions for the parachute descent phase, the maximum reachable range $S_{\max}$ and minimum reachable range $S_{\min}$ is computed by the extreme-range optimization model

$$\begin{cases} S_{\max} = Q_{\max}(h_{\mathrm{p}i}, v_{\mathrm{p}j}, \gamma_{\mathrm{p}k}) \\ S_{\min} = Q_{\min}(h_{\mathrm{p}i}, v_{\mathrm{p}j}, \gamma_{\mathrm{p}k}) \end{cases} \tag{17}$$

where $Q_{\max}$ and $Q_{\min}$ are the maximum-range and minimum-range optimization model, respectively.

The multi-dimensional parachute deployment box W_2 incorporating altitude, velocity, flight-path angle, and extreme range is constructed

$$W_2 = \{(h_{\mathrm{p}i}, v_{\mathrm{p}j}, \gamma_{\mathrm{p}k}, S_{\max}, S_{\min})\} \tag{18}$$

2.3 Control logic for Parachute Deployment

A control logic for parachute deployment is developed based on a multi-dimensional parachute deployment box to balance the requirements of safe parachute deployment and precise landing.

Based on the multi-dimensional parachute deployment box, the extreme-range interpolation functions $f_1(\cdot)$ and $f_2(\cdot)$ are constructed to yield the maximum reachable range $S_{\max}$ and minimum reachable range $S_{\min}$ under current states (h, v, γ). Linear interpolation is adopted as the interpolation methodology. The interpolation functions are expressed as

$$\begin{cases} S_{\max} = f_1(h, v, \gamma) \\ S_{\min} = f_2(h, v, \gamma) \end{cases} \tag{19}$$

The evaluation index for landing precision is designed, as shown in Equation (20)

$$J = \left| S_{\mathrm{go}} - \frac{S_{\max} + S_{\min}}{2} \right| \tag{20}$$

where S_{go} is range-to-go, which is defined as the great-circle distance from the lander's current position to the target landing site

$$S_{\mathrm{go}} = R_0 \arccos[\cos\phi \cos\phi_{\mathrm{f}} \cos(\theta - \theta_{\mathrm{f}}) + \sin\phi \sin\phi_{\mathrm{f}}] \tag{21}$$

where R_0 is the radius of the Mars, θ_{f} is the longitude of the target landing site, and ϕ_{f} is the latitude of the target landing site.

The evaluation index quantifies the proximity between the range-to-go S_{go} and the midpoint of the reachable range interval $[S_{\min}, S_{\max}]$. A reduced J value demonstrates improved convergence characteristics, indicating that parachute deployment under such conditions maximizes landing accuracy with less fuel consumption.

Based on the foregoing analysis, the control logic for parachute deployment is formulated as

$$\xi = \begin{cases} 1, & \text{if } J(S_{\mathrm{go}}) = \min J \text{or} (\boldsymbol{X}_t \in W_2 \text{ and } \boldsymbol{X}_{t+1} \notin W_2) \\ 0, & \text{otherwise} \end{cases} \tag{22}$$

where ξ denotes the parachute deployment parameter. $\xi = 1$ corresponds to parachute deployment and $\xi = 0$ corresponds to no parachute deployment.

In conclusion, the parachute deployment process based on the multi-dimensional box is demonstrated as follows: At the terminal of the entry descent phase, upon the lander's states satisfy the classical two-dimensional box, the maximum reachable range $S_{\max}$ and minimum reachable range $S_{\min}$ are computed in real-time based on the lander's states and the extreme-range interpolation function presented in Equation (19). Simultaneously, the evaluation index of landing precision defined in Equation (20) is computed online. The parachute deployment is triggered under one of criteria given by Equation (22): 1) When the evaluation index J is minimized (i.e., the index at the subsequent time step is larger than that at the preceding one), parachute deployment is triggered as the range-to-go S_{go} is close to the midpoint of the reachable range interval $[S_{\min}, S_{\max}]$. 2) If the evaluation index J is still decreasing but the lander's states are about to breach the multi-dimensional box (i.e., exceed the edge of the constraint envelope), parachute deployment is enforced to ensure safety. Parachute deployment should not be triggered under all other circumstances. The parachute deployment triggering criteria are evaluated at each control cycle throughout the terminal of the entry phase until the parachute deployment is triggered.

3 Simulations

A landing mission of the Mars is considered to verify the multi-dimensional parachute deployment box. For simulation comprehensiveness, two distinct sets of initial conditions were configured to facilitate subsequent selection in simulation runs, as presented in Table 1. The maximum and minimum thrust magnitude are 26 516 N and 9 944 N, respectively. The gravitational acceleration on Mars is 3.72 m/s^2. The bank angle is assumed to be zero at the terminal of the entry phase. Other parameters and constraints are given by Table 2.

Table 1 Initial conditions of Mars lander at entry terminal

Parameter	Case 1	Case 2
Longitude/(°)	0	0
Latitude/(°)	0	0
Altitude/km	12	8
Velocity/(m·s^{-1})	500	500
Flight-path angle/(°)	–10	–10
Range-to-go/km	15	18

Table 2 Parameters and constraints for Mars lander

Parameter	Value
m_0/kg	4 100
m_{h}/kg	400
m_{b}/kg	400
m_{fuel}/kg	500
$M_{\max}$	2.2
$M_{\min}$	1.4
$q_{\max}$ /Pa	850
$q_{\min}$/Pa	300
$h_{\min}$/km	6
v_{h}/(m·s^{-1})	140
h_{T}/km	2

3.1 Results of Multi-dimensional Box

The multi-dimensional parachute deployment box is constructed based on the extreme-range optimization model. The initial conditions of the lander are set as Case 1. The landing trajectories with the extreme range are given in Fig. 2. The difference between two trajectories is

originated from the powered descent phase because the lander has no control authority during the parachute descent phase. Under such parachute deployment states, the extreme ranges of the lander are 4.82 km and 12.06 km. In other words, the lander's reachable range is constrained to the interval [4.82 km, 12.06 km].

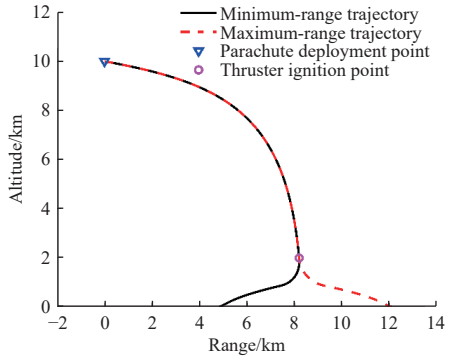

Fig. 2　Landing trajectories with extreme range

The multi-dimensional parachute deployment box is shown in Fig. 3. For the convenience of presentation, only the flight-path angle and range dimensions at the velocity-altitude coordinate of (400 m/s, 10 km) are presented. This multi-dimensional box displays the lander's reachable range interval after parachute deployment under specified deployment states (h, v, γ).

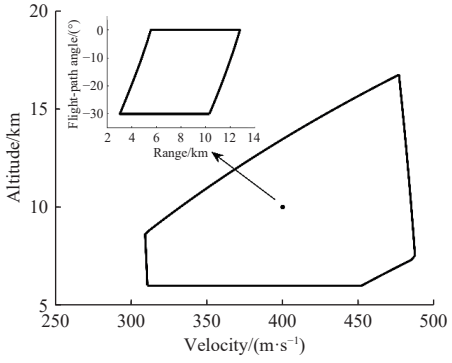

Fig. 3　Multi-dimensional parachute deployment box

3.2　Landing Results in Nominal Case

To validate the effectiveness of the proposed multi-dimensional box on parachute deployment control, simulations were conducted in two nominal cases presented in Table 1.

Fig. 4 demonstrates the range-to-go profile at the terminal of the entry phase in Case 1. Note that the computation of extreme range and evaluation index is initiated upon the lander's entry into the two-dimensional box, thus the recording of S_{max} and S_{min} commences solely subsequent to t = 4 s. At t = 4 s, the range-to-go is within the extreme range and the deployment safety is guaranteed, yet the evaluation index had not reached its minimum value. At t = 13 s, the evaluation index attained its minimum value while the lander remained within the multi-dimensional deployment box. Subsequently, parachute deployment is triggered, initiating the lander's transition into the parachute descent phase. This is in accord with the first criterion of the control logic for parachute deployment.

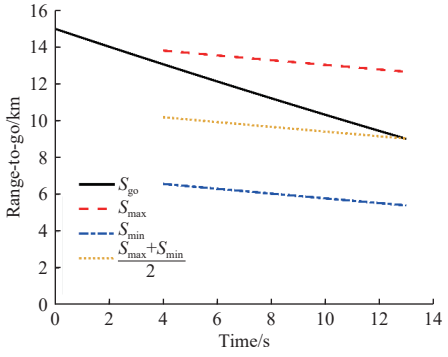

Fig. 4　Range-to-go profile in Case 1

The altitude-velocity profile of the lander in Case 1 is illustrated in Fig. 5. Initially, the lander's state remains outside the two-dimensional box, indicating an unsafe condition for parachute deployment. Entering the two-dimensional box at t = 4 s, parachute deployment is still withheld due to the non-optimal evaluation index. Parachute deployment is triggered at 10.68 km altitude and 438.27 m/s velocity (t = 13 s), within the validated safe deployment boundaries.

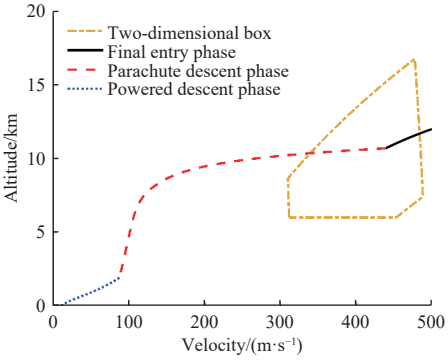

Fig. 5　Altitude-velocity profile in Case 1

Fig. 6 shows the range-to-go profile at the terminal of the entry phase in Case 2. Initially, the lander's state

remains outside the two-dimensional box. At t = 2 s, the lander enters the two-dimensional box but remains outside the multi-dimensional box, as the range-to-go exceeds the maximum reachable range. At t = 19 s, the lander enters the multi-dimensional deployment box, while the evaluation index J is continuously decreasing. At t = 22 s, parachute deployment is triggered although the evaluation index does not reach its minimum value. This can be attributed to the fact that lander's states are about to breach the two-dimensional box, which is in accordance with the second criterion of the control logic for parachute deployment.

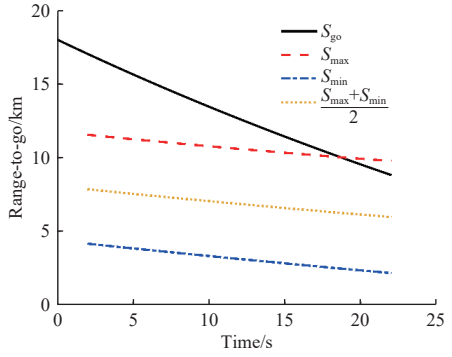

Fig. 6 Range-to-go profile in Case 2

The altitude-velocity profile of the lander in Case 2 is presented in Fig. 7. Initially, the lander's states remain outside the two-dimensional box. Computation of the evaluation index is initiated subsequent to the lander's entry into the two-dimensional box. At t = 22 s, the lander's states are at the edge of the two-dimensional box. For safety reason, the parachute deployment is triggered.

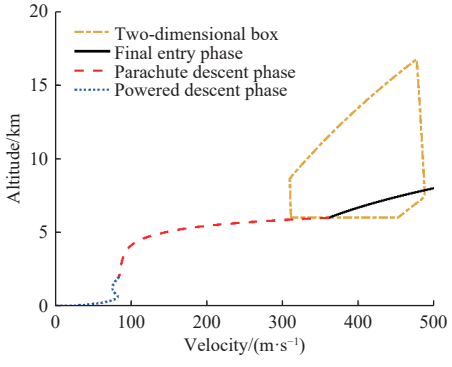

Fig. 7 Altitude-velocity profile in Case 2

To verify the capability of controlling the range-to-go, the multi-dimensional parachute deployment box is compared with two existing parachute deployment methods. Method 1 employs the classical two-dimensional box. Once the lander enters this box, the parachute deployment is triggered. Method 2 triggers the parachute deployment when the lander's velocity drops below 450 m/s or its altitude drops below 7 km[23-24]. Method 3 utilizes the proposed multi-dimensional box. Figs. 8–9 present landing trajectories for various methods. In Case 1, all landers achieve precise landing. The lander utilizing Method 1 triggers the parachute deployment earlier, leading to a 13.6% increase in fuel consumption during the powered descent phase to eliminate the range-to-go error. The early deployment is due to the absence of range information in two-dimensional box. Similarly, Method 2 resulted in a 1.03% increase in fuel consumption. In Case 2, the range-to-go at the terminal of the entry phase is larger than that in Case 1. Both Method 1 and Method 2 fail to deliver the lander to the target location. Conversely, the lander utilizing Method 3 achieved precise landing at the target position. Therefore, the proposed multi-dimensional box exhibits remarkable range control capability, facilitating significant conservation of fuel consumption during the subsequent powered descent phase.

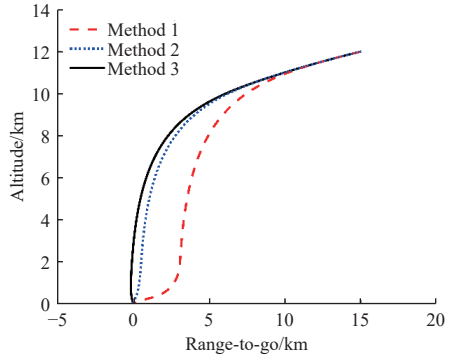

Fig. 8 Landing trajectories for various methods in Case 1

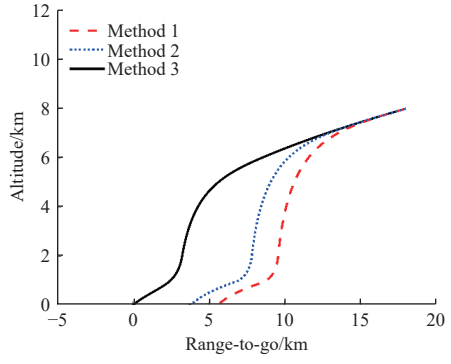

Fig. 9 Landing trajectories for various methods in Case 2

3.3 Landing Results in Dispersed Cases

To verify the capability of eliminating the range-to-go error, three methods under disturbances are simulated by Monte Carlo method with 500 runs. There exist disturbances in the initial range-to-go of the lander, following a zero-mean Gaussian distribution with the three-standard deviation being 10 km. The landing trajectories are given in Figs. 10–12. Both Method 1 and Method 2 neglect range information, resulting in residual range-to-go errors and poor landing accuracy. Precise landing is achieved by only 54.2% and 73.4% of landers employing Method 1 and Method 2, respectively. In contrast, 96% of landers utilizing Method 3 successfully reached the designated landing site, demonstrating robust range control capability and high landing precision compared with the other two methods. Therefore, the multi-dimensional box effectively eliminates the range-to-go error and exhibits range control capability.

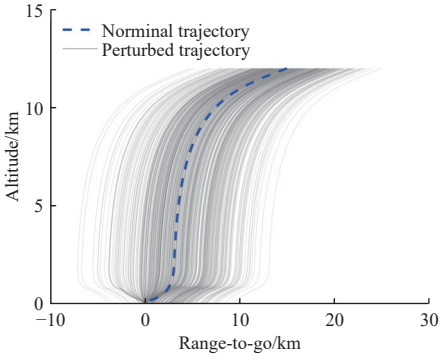

Fig. 10　Landing trajectories for Method 1 in dispersed cases

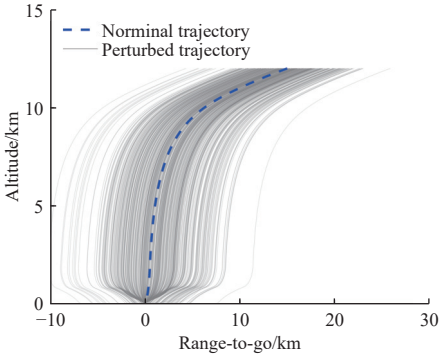

Fig. 11　Landing trajectories for Method 2 in dispersed cases

The terminal range errors, defined as the distance between the actual and designated landing sites, are illustrated in Table 3. Both the mean and maximum terminal landing errors for Methods 1 and 2 significantly exceed those of Method 3. The reduced error is attributable to the range-based parachute deployment logic. Therefore, the multi-dimensional parachute deployment box provides the lander with the superior range control capability.

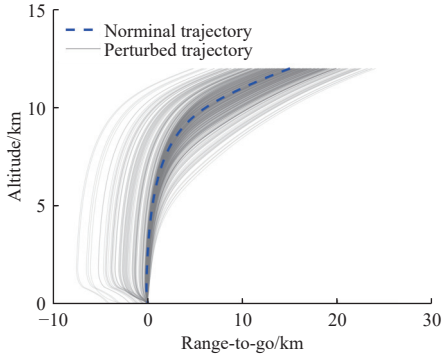

Fig. 12　Landing trajectories for Method 3 in dispersed cases

Table 3　Terminal range errors of three methods

Parameter	Method 1	Method 2	Method 3
Mean error/km	1.18	0.47	0.05
Maximum error/km	9.30	7.53	4.13

4　Conclusion

A multi-dimensional parachute deployment box for Mars landing has been developed, aiming at both parachute deployment safety and landing precision. The proposed box is constructed on the basis of the extreme-range optimization model and the two-dimensional box, where the former introduced the range information and the latter guaranteed the safety. An evaluation index of range control capability is formulated, and the control logic for parachute deployment is developed. The simulation results demonstrate that the proposed multi-dimensional box satisfies the requirements of safe parachute deployment and accurate landing, exhibiting superior landing precision compared to the classical two-dimensional box. Meanwhile, the multi-dimensional box effectively eliminates the range-to-go error at the terminal of the entry phase and improves the range control authority, proving its applicability for Mars landing missions.

References

[1] CUI P, ZHAO D, ZHU S. Obstacle avoidance guidance for planetary landing using convex trajectory and adaptive curvature regulation[J]. Acta Astronautica, 2022, 199: 313-326.

[2] CUI P, LONG J, ZHU S, et al. Research progress of planetary landing trajectory optimization techniques[J]. Journal of Astronautics, 2021, 42(6): 677-686.

[3] LU P，SANDOVAL S，DAVAMI C. Fast and robust optimization of full trajectory from entry through powered descent[J]. Journal of Guidance，Control，and Dynamics，2024，47(2)：203-216.

[4] HUANG X，XU C，GUO M. Research progress of autonomous navigation and control technology for extraterrestrial soft landing[J]. Journal of Deep Space Exploration，2024，11(1)：3-15.

[5] GONG Y，GUO Y，LI D，et al. Fixed-time planetary landing guidance with unknown disturbance and thruster constraint[J]. IEEE Transactions on Aerospace and Electronic Systems，2023，59(1)：483-496.

[6] LONG J，GAO A，CUI P. Lateral predictive guidance for Mars atmospheric entry[J]. Journal of Deep Space Exploration，2016，3(2)：145-149，180.

[7] RAO W，SUN Z，MENG L，et al. Analysis and design for the Mars entry，descent and landing mission[J]. Journal of Deep Space Exploration，2016，3(2)：121-128.

[8] GUO M，LI M，HUANG X，et al. On guidance algorithm for martian atmospheric entry in nonconforming terminal constraints[J]. Journal of Deep Space Exploration，2017，4(2)：184-189.

[9] GUO M，HUANG X，LI M，et al. Adaptive entry guidance for the Tianwen-1 mission[J]. Astrodynamics，2022，6(1)：17-26.

[10] LIANG Z，MEASE K D. Precision guidance for Mars entry with a supersonic inflatable aerodynamic decelerator[J]. Journal of Guidance，Control，and Dynamics，2019，42(7)：1571-1578.

[11] SUN Z. Technology of deep space exploration[M]. Beijing：Beijing Institute of Technology Press，2018.

[12] DONG J，RAO W，SUN Z，et al. Interdisciplinary design and validation for key phases of martian landing missions[J]. Journal of Astronautics，2022，43(1)：21-29.

[13] INGOLDBY R N. Guidance and control system design of the viking planetary lander[J]. Journal of Guidance and Control，1978，1(3)：189-196.

[14] PRINCE J L，DESAI P N，QUEEN E M，et al. Entry，descent，and landing operations analysis for the Mars Phoenix lander[J]. Journal of Spacecraft and Rockets，2011，48(5)：778-783.

[15] KIPP D，MARTIN M S，ESSMILLER J，et al. Mars Science Laboratory entry，descent，and landing triggers[C]//Proceedings of 2007 IEEE Aerospace Conference. MT，USA：IEEE，2007.

[16] CRUZ J R，WAY D W，SHIDNER J D，et al. Reconstruction of the Mars science laboratory parachute performance[J]. Journal of Spacecraft and Rockets，2014，51(4)：1185-1196.

[17] CLARK I G，O'FARRELL C，KARLGAARD，C D. Reconstructed performance of the supersonic parachute of the Mars InSight lander[J]. Journal of Spacecraft and Rockets，2021，58(6)：1601-1611.

[18] HUANG X，XU C，GUO M，et al. Tianwen-1 entry，descent，and landing guidance，navigation，and control system design and validation[J]. Journal of Spacecraft and Rockets，2023，60(6)：1983-2002.

[19] O'FARRELL C，CLARK I G. Reconstructed performance of Mars 2020 parachute decelerator system[J]. Journal of Spacecraft and Rockets，2024，61(5)：1313-1328.

[20] NELESSEN A，SACKIER C，CLARK I，et al. Mars 2020 entry，descent，and landing system overview[C]//Proceedings of 2019 IEEE Aerospace Conference. MT，USA：IEEE，2019.

[21] DONG J，RAO W，SUN Z，et al. Multibody dynamics characteristics analysis and safety design research of the Mars parachute descent process[J]. Scientia Sinica Technologica，2022，52(8)：1175-1185.

[22] ACIKMESE B，CARSON J，BLACKMORE L. Lossless convexification of nonconvex control bound and pointing constraints of the soft landing optimal control problem[J]. IEEE Transactions on Control Systems Technology，2013，21(6)：2104-2113.

[23] SHEN G，XIA Y，SUN H. A 6DOF mathematical model of parachute in Mars EDL[J]. Advances in Space Research，2015，55(7)：1823-1831.

[24] XIA Y，CHEN R，PU F，et al. Active disturbance rejection control for drag tracking in Mars entry guidance[J]. Advances in Space Research，2014，53(5)：853-861.

The Author Profiles

XING Zhehao(2001−)，male，doctoral candidate，research areas：trajectory optimization，guidance and control for spacecraft.

Address：No.5 Zhongguancun South Street，Haidian District，Beijing Institute of Technology (100081)

TEL：18935182011

E-mail：xzh@bit.edu.cn

LIANG Zixuan(1988−)，male，professor，research areas：trajectory optimization，guidance and control for spacecraft，exploration and defense for asteroid. **Corresponding author of this article**.

Address：No.5 Zhongguancun South Street，Haidian District，Beijing Institute of Technology (100081)

TEL：(010)68913550

E-mail：liangzx@bit.edu.cn

面向火星精确着陆的多维开伞窗口设计

邢哲豪[1,2]，梁子璇[1,2]

（1. 北京理工大学 空天科学与技术学院，北京，100081；
2. 深空自主技术工业和信息化部重点实验室，北京 100081）

摘　要：在火星着陆任务中，进入段结束的减速伞开伞时机对着陆位置精度具有重要影响。本文针对安全开伞和精确着陆需求，提出了一种用于判定火星着陆开伞条件的多维开伞窗口。首先，综合伞降段和动力下降段的动力学与约束，建立了火星着陆器开伞后的极限航程优化模型。接着，在高度–速度二维开伞窗口的基础上，融合了极限航程信息，构建了高度、速度、航迹角、极限航程表征的多维开伞窗口。在此基础上，设计了落点精度评价指标，提出了落点偏差最小的开伞控制策略。最后，结合火星着陆任务，对所提出的多维开伞窗口进行仿真。结果表明，多维开伞窗口能够兼顾安全开伞与精确着陆需求，可以通过控制开伞时机有效消除进入末段的待飞航程误差。

关键词：火星探测；精确着陆；多约束；开伞窗口；开伞控制

[责任编辑：宋宏，英文审校：宋利辉]